Cutting Force Dynamics as a Tool for Surface Profile Monitoring in AWJ

R. Kovacevic
Member ASME

R. Mohan
Student Member ASME

Y. M. Zhang
Member ASME

Center for Robotics and
Manufacturing Systems and
Department of Mechanical Engineering,
University of Kentucky,
Lexington, KY 40506

Abrasive waterjet cut surface is characterized using static and dynamic characterization techniques. A novel method of auto regressive moving average model identification called model distance method is utilized here for surface profile and dynamic force characterization. More information about the surface profile generating mechanism is derived through wavelength decomposition of the ARMA models. The dynamic workpiece normal force in abrasive waterjet is influenced by process parameters such as fluctuations in water pressure, change in abrasive flow rate, vibration of the positioning system, traverse speed, nozzle diameter, etc. An attempt has been made in this paper to link the dynamics of the process to the quality of the generated surface. The feasibility of using the dynamic workpiece normal force as a parameter for on-line monitoring of the surface profile generated by abrasive waterjet is also investigated.

1 Introduction

Abrasive waterjet (AWJ) cutting technique can be considered as one of the most recent nontraditional manufacturing processes to be introduced. In this technique, the material removal is primarily through the erosive action of abrasive particles which are accelerated by a thin stream of high velocity waterjet and are directed through an AWJ nozzle. AWJ cutting was first introduced as a commercial system in 1983 for cutting glass. Nowadays, this process is being used widely for machining hard to machine materials like ceramics, ceramic composites, metal matrix composites, laminates, fiber re-inforced resin composites, titanium and its alloys, etc., where conventional machining is often not technically or economically feasible. High speed and multidirectional cutting capability, high cutting efficiency, ability to cut complicated shapes of even nonflat surfaces very effectively at close tolerances, easy accomplishment of changeover of cutting patterns under computer control, etc., are a few of the advantages offered by this process which make it ideal for a flexible manufacturing environment.

In AWJ cutting, as the jet penetrates into the workpiece, it loses its kinetic energy continuously and starts deflecting. Thus typically, the surface produced by AWJ has two distinct regions along the kerf; one is a relatively smooth region (cutting wear zone) at the top of the kerf and the other a striated region (deformation wear zone) at the bottom of the kerf. In order to achieve the desired surface finish, the AWJ cutting process needs to be monitored on-line and controlled through a closed-loop feedback and control system. Characterization of the surface profiles generated by AWJ under various cutting conditions will give us information about how to control the process. We know that the kinematics as well as the dynamics of the cutting process are responsible for the surface profile generating mechanism in jet cutting processes. Dynamic characterization of the surface profile will give us information about the mechanism of surface profile generation and clues about the influence of cutting parameters on the generated surface profile.

Characterization of surface profiles generated by AWJ has been studied by several investigators [1–6]. The concept of cutting wear mode and deformation wear mode as applicable to AWJ generated surfaces were introduced [7] by Hashish. Through a separate investigation, Chao et al. [8] established that there is a strong correlation between the nozzle vibration and the waviness of AWJ generated surface. Hashish developed a physical model [9] to describe the waviness (striations) phenomenon associated with AWJ cutting. The quantitative discrepancies observed in the model were attributed to kerf taper effects. The present authors have characterized [10] the surface texture generated by AWJ cutting and laser machining by stochastic modeling of large sample size data for a comparative study. Several studies have been conducted in AWJ cutting to establish correlation between workpiece normal force generated by the AWJ and surface texture [11–15].

Various methods have been adopted for characterization of surface profiles generated by different manufacturing processes, through static parameters [16–17]. Although the computation of the static parameters is straightforward, they may not reflect the peculiarities of the profile generating process due to their empirical nature. It can also be noted that there is a considerable overlap of these parameter values for various machining processes. Assessment of surface typology analysis techniques [18] reveal that there is a need for more

Contributed by the Production Engineering Division for publication in the JOURNAL OF ENGINEERING FOR INDUSTRY. Manuscript received April 1993; revised July 1994. Associate Technical Editor: K. Rajurkar.

detailed comprehensive analyses. Time series analysis offers a surface characterization technique which can readily relate to the dynamics of the manufacturing process generating the surface profile. There have been several studies of dynamic characterization of surface profile data through the dynamic data system (DDS) modeling technique [19–27].

From the review of the work already done it can be noted that:

- AWJ cutting system generates striated surfaces which can be modeled using stochastic modeling technique.
- Stochastic model characterization as a dynamic modeling technique has provided insight into the high energy jet cutting processes.
- However, in previous modeling of surfaces, data sets having only a few hundreds of observations have been utilized to fit auto regressive moving average (ARMA) models due to extensive computational burden of conventional modeling approaches. As a result, inaccurate models are frequently obtained.
- Workpiece normal force (static) has been found to be a good indicator of the surface profile generated by AWJ.
- But no study on the dynamic portion of the cutting force was conducted to extract information about the surface profile.

In AWJ cutting, once the striations begin to appear along the kerf, the surface finish is predominantly decided by presence of striations (waviness). Hence the objective of this study is to investigate the role played by the cutting parameters in the striation generating mechanisms of AWJ cutting process. The dynamic workpiece normal force in AWJ is influenced by process parameters such as fluctuations in water pressure, change in abrasive flow rate, vibration of the positioning system, traverse speed, nozzle diameter, etc. An attempt has been made in this paper to link the dynamics of the process to the quality of the generated surface. The focus will be on investigating the feasibility of using dynamic workpiece normal force as a parameter for on-line monitoring of surface profile generated by AWJ. A new approach called model distance method [28] is employed for stochastic modeling of large sample sizes of surface profile data and dynamic force data. As the same surface has regions where striations are present and absent, the terms "roughness" and "waviness" are used interchangeably here. In other words, for a striated surface, the term "surface roughness" indicates "surface waviness" in the very strict sense.

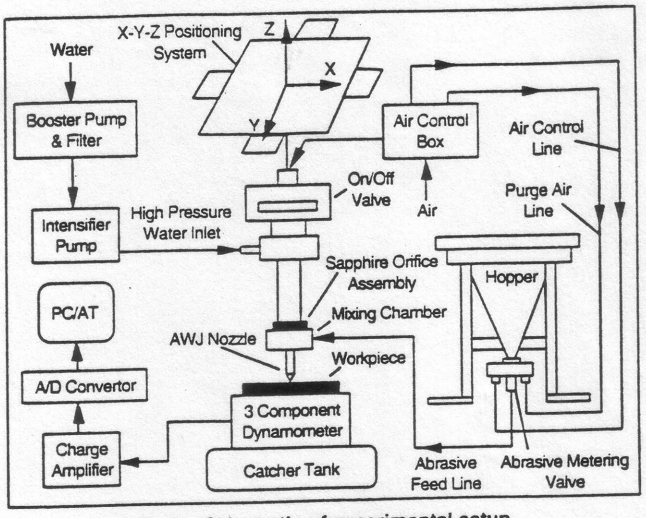

Fig. 1 Schematic of experimental setup

Table 1 Process parameters

Abrasive Waterjet Cutting	
Abrasive material	- Garnet
Abrasive mesh size	- 80 (0.180 mm)
Abrasive particle shape	- angular(random)
AWJ orifice material	- Sapphire
AWJ orifice diameter	- 0.254 mm
Mixing nozzle length	- 76.2 mm
Mixing nozzle diameter	- 0.762 mm
Method of feed	- suction
Condition of abrasive	- dry
Angle of Jet	- 90 degrees
Workpiece Details	
Material	- Aluminum Al 2024
Material thickness	- 25.4 mm
Length of cut	- 50.8 mm
Experimental Variables	
Range of Waterjet Pressure	- 248 MPa to 331 MPa
Range of Stand-off Distance	- 5.08 mm to 12.70 mm
Range of Traverse Speed	- 0.42 mm/s to 1.69 mm/s
Range of Abrasive Flow Rate	- 2.27 g/s to 4.54 g/s

2 Experimental Setup and Procedure

The experimental setup consists of an AWJ cutting system, a three component dynamometer, charge amplifier, A/D convertor, PC/AT with suitable software and workpiece. The AWJ cutting system used for conducting the experiment consists of a high pressure intensifier pump, abrasive metering and delivery system, AWJ cutting head, catcher tank and X-Y-Z positioning table controlled by a CNC controller. A schematic of the experimental setup is shown in Fig. 1. The workpiece used here is aluminum, Al 2024 of 25.4 mm thickness. A thick workpiece is chosen to study the variation of surface finish along the kerf wall. The parameters of AWJ cutting chosen for evaluation are water pressure, stand-off distance, traverse speed and abrasive flow rate as they are found to be the most influential on the surface profile. The process parameters for this experiment are given in Table 1.

The workpiece is kept on a dynamometer to measure the workpiece normal force which indirectly gives the normal force exerted by the impacting AWJ while cutting. The dynamic component of the force is taken for analysis. The cutting parameters were chosen at four different levels so that the influence of each parameter on the surface profile could be studied separately. However, the minimum level of each cutting parameter is selected to ensure through-cutting of the workpiece. Different samples were cut by AWJ for a length of about 50 mm by varying each cutting parameter and keeping the other parameters constant at their mean value. The profile of the cut surface was measured using a profilometer at three different levels along the kerf; one at about 2.5 mm from the top surface, where the striations are not present (cutting wear zone—level "a"), one at the zone where the striations start to appear (transition zone—level "b") and the third at about 2.5 mm from the bottom surface, where the striations dictate the surface finish (deformation wear zone—level "c"). To eliminate the effects of the entry stage and exit stage of the cutting process, the surface profile is measured at the middle of the cut for a length of about 40 mm. Typical surface profiles generated at levels a, b & c are given in Fig. 2. Surface roughness parameters like roughness average (R_a), skewness (R_{sk}), and kurtosis (R_{ku}) which indicate the static characteristics of the surface profile, are also measured.

The ASCII file of each surface profile data set used for stochastic modeling consisted of about 7,500 observations at a sampling interval of 5 μm. Considering the measuring speed of 0.5 mm/s, this represents a sampling frequency of

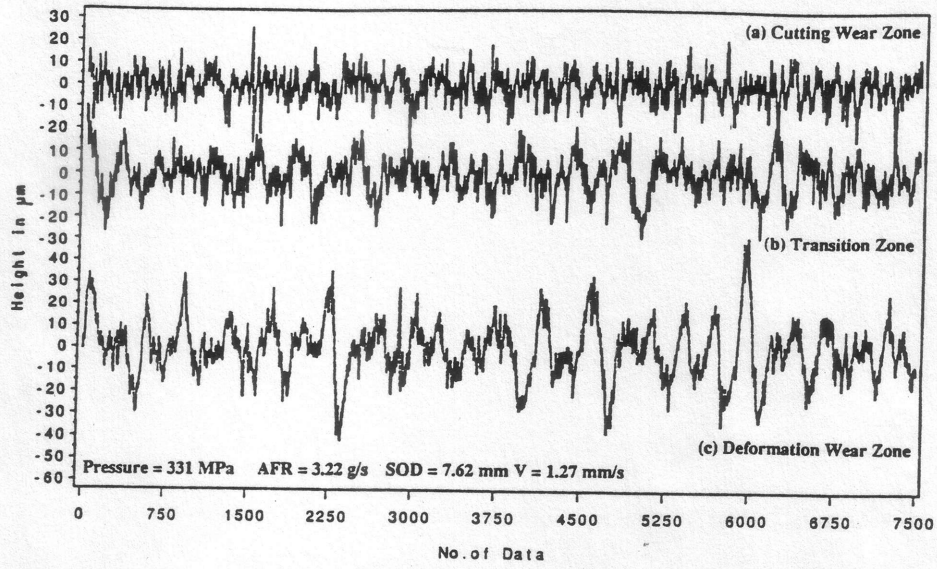

Fig. 2 Typical surface profiles generated by AWJ

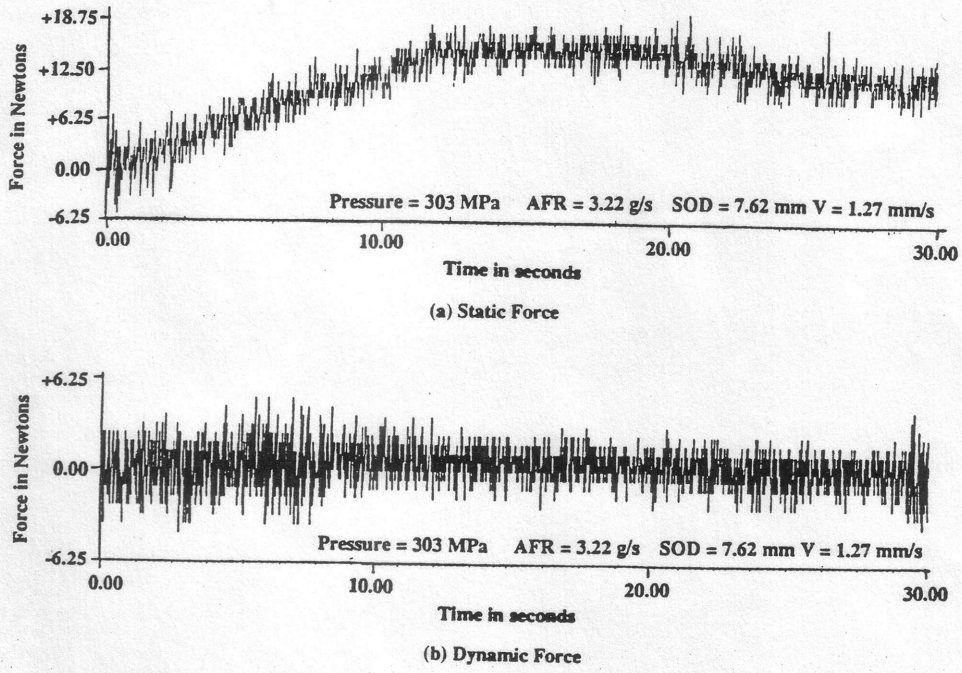

Fig. 3 Typical cutting force signals, (*a*) static force, (*b*) dynamic force

100 Hz. The number of data points (per data set) used here is much larger than that used for similar work in this area which is of the order of only a few hundred [24]. Each dynamic force data set consisted of about 4000 observations at a sampling frequency of 100 Hz. Typical static cutting force signal and the corresponding dynamic force signal are given in Figs. 3(*a*) and (*b*), respectively. The dynamic force signal has been utilized in this paper for ARMA modeling.

Each data set (of both surface profile as well as dynamic force) is fitted with suitable ARMA model using the model distance approach [28]. Even though ARMA modeling has been verified to be an effective tool for characterization of various engineering surfaces, there is no suitable approach for selecting an optimum sampling interval for ARMA characterization. Moreover, the accuracy requirement varies from case to case. Hence more data is expected to be processed for more accurate results. The computational burden prevents one from selecting extensive data. As a matter of fact, since the parameter estimation of the ARMA models is nonlinear, and since the computational burden of the conventional methods (for example, the nonlinear least squares (NLS) method [29] and maximum likelihood (ML) method [30]) are proportional to the sample sizes, the identification of large samples will be time consuming. Therefore an alternative algorithm for identifying ARMA models has been proposed [28] based on the concept of model distance.

3 ARMA Modeling Using Model Distance Approach

The aim of this approach is to increase the ratio of accuracy to computational burden, with reliable evaluation of the final modeling accuracy. The proposed approach consists of a two step procedure:

(*1*) AR modeling—Identifying an AR model from the samples.

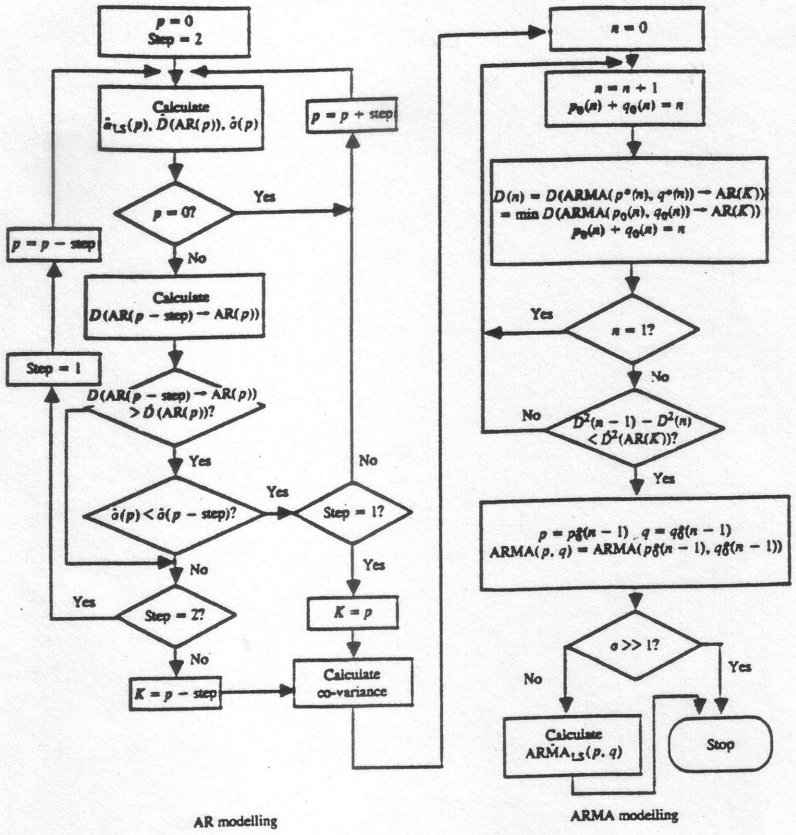

$\hat{a}_{LS}(p)$ parameter estimate vector of AR(p)
$\hat{\sigma}(p)$ standard deviation estimate of AR(p) modelling residual
$\hat{D}$(AR(p)) parameter estimate error (measured in the model distance)
$D(M_1 \rightarrow M_2)$ model distance from M_1 to M_2
AR(K) selected AR model

Fig. 4 Procedure of ARMA modeling by model distance method

(2) ARMA approximation—Identifying the ARMA model based upon this AR model.

It has been shown that, by this method, the ratio of modeling accuracy to computational burden increases with sample size, whereas this ratio is nearly constant for conventional methods. Also, its computational burden is nearly independent of sample size. This makes it possible for us to adequately utilize extra samples to improve the modeling accuracy without a virtual increase in computational burden. ARMA models will be identified here using this approach. The flow chart in Fig. 4 gives the outline of this procedure. The method is briefly described below:

Suppose the sample of y_t is produced from:

$$M: \quad \phi(B)y_t = \theta(B)\varepsilon_t \tag{3.1}$$

where M is a notation for the model (3.1), B is the backshift operator, $\varepsilon \sim N(0, \sigma_\varepsilon^2)$, and

$$\phi(B) = 1 - \sum_{j=1}^{p} \phi_j B^j, \quad \theta(B) = 1 - \sum_{j=1}^{q} \theta_j B^j$$

where ϕ_j and θ_i ($j = 1, \ldots, p$; $i = 1, \ldots, q$) are real.

Suppose $\hat{M}$ (ARMA ($\hat{p}$, $\hat{q}$)) is an estimate of M:

$$\hat{M}: \quad \hat{\phi}(B)y_t = \hat{\theta}(B)\hat{\varepsilon}_t \tag{3.2}$$

where $\hat{\varepsilon}_t$ is the residual of $\hat{M}$, and

$$\hat{\phi}(B) = 1 - \sum_{j=1}^{\hat{p}} \hat{\phi}_j B^j \quad \hat{\theta}(B) = 1 - \sum_{j=1}^{\hat{q}} \hat{\theta}_j B^j$$

where $\hat{\phi}_j$ and $\hat{\theta}_i$ ($j = 1, \ldots, \hat{p}$; $i = 1, \ldots, \hat{q}$) are real.

First-order model distance from $\hat{M}$ to M can be defined as

$$D_1(\hat{M} \rightarrow M) \equiv \sqrt{\frac{E_1(\hat{M}) - E_1(M)}{E_1(M)}} = \sqrt{\frac{\Delta E_1(\hat{M} \rightarrow M)}{\sigma_\varepsilon^2}} \tag{3.3}$$

where, $E_1(M)$ ($E_1(\hat{M})$) is the variance of the *one-step-ahead* prediction error when the minimum mean squared forecast is performed using M ($\hat{M}$). Suppose M, $\hat{M}$ assume the following AR model forms:

$$M: \quad y_t = \sum_{j=1}^{\infty} a_j y_{t-j} + \varepsilon_t, \quad \hat{M}: \quad y_t = \sum_{j=1}^{\infty} \hat{a}_j y_{t-j} + \hat{\varepsilon}_t \tag{3.4}$$

It can be shown:

$$\Delta E_1(\hat{M} \rightarrow M) = \Delta a^T R \Delta a \tag{3.5}$$

where $\Delta a = (\Delta a_1, \Delta a_2, \ldots, \Delta a_L)^T = (a_1 - \hat{a}_1, a_2 - \hat{a}_2, \ldots, a_L - \hat{a}_L)^T$, $R_{L\times L}(i, j) = \gamma(|j - i|) = E(y_{t-i}y_{t-j})$, and L ($L \gg m$) is a positive infinite integer (which can be taken to be a sufficiently large integer in numerical computation). $\gamma(j)$ can be calculated based upon both ϕ_j, θ_i ($j = 1, \ldots, p$ $i = 1, \ldots, q$) and σ_ε^2 [29].

Let us assume that we have model $AR(p_1)$ having less parameters than model $AR(p_2)$. If $D(AR(p_2)) < D(AR(p_1) \rightarrow AR(p_2))$ and $\hat{\sigma}_\varepsilon^2(AR(p_2)) < \hat{\sigma}_\varepsilon^2(AR(p_1))$, select $AR(p_2)$; otherwise, do not select $AR(p_2)$. This criterion of prediction is corresponding to the least squares estimation.

Let us discuss the computation of $D(AR(p_2))$. Assume an AR model to be described by $\phi_j's (j = 1, 2, \ldots, p)$ and its estimate $\widehat{AR}$ by $\hat{\phi}_j's (j = 1, 2, \ldots, p)$. It can be shown that

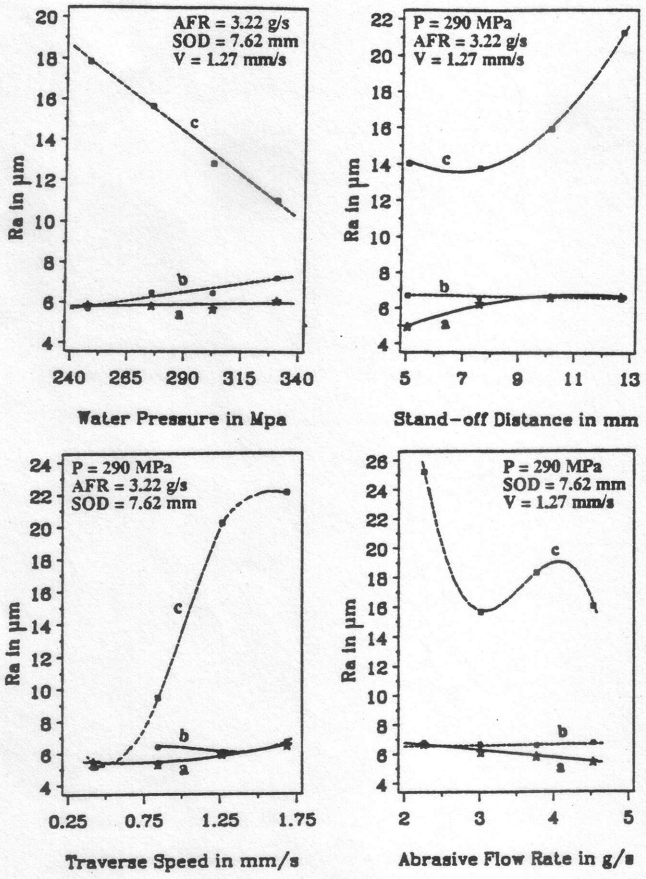

(a) Cutting wear zone (b) Transition zone (c) Deformation wear zone

Fig. 5 Plot of surface roughness (R_a) vs cutting parameters

$$\Delta E_1(\widehat{AR} \rightarrow AR) \equiv F = \sum_{i=1}^{p} \sum_{j=1}^{p} \Delta\phi_i \Delta\phi_j \gamma(|i-j|) \quad (3.6)$$

Thus, the corresponding model distance $D(\widehat{AR} \rightarrow AR)$ can be calculated.

As it is impossible to find the values of $\phi_j's$ and $\hat{\phi}_j's$ during modeling and since actual parameter values are not available, an approximation of $\Delta E_1(\widehat{AR})$ which is more practical as an estimate of the modeling accuracy than $\Delta E_1(\widehat{AR} \rightarrow AR)$ is given by,

$$\Delta \hat{E}_1(\widehat{AR}) = \Delta E_1(\widehat{AR})|_{\widehat{AR}} = \sum_{i=1}^{p} \sum_{j=1}^{p} V_{\phi\phi}(i,j)\hat{\gamma}(|i-j|) \quad (3.7)$$

where $\hat{\gamma}$ is calculated based upon $\widehat{AR}$.

The method of calculation of accuracy of this approximation is given in [28]. The resulting AR model can be represented by AR(K).

As AR(K) is an adequate representation of the samples, parameters of ARMA(p, q) can be acquired based upon the following criterion;

$$\hat{\phi}^*, \hat{\theta}^*: \min_{\hat{\phi} \in R^p, \hat{\theta} \in R^q} D_1^2\left((\hat{\phi}, \hat{\theta}) \rightarrow \alpha\right) \equiv \min_{\hat{\phi} \in R^p, \hat{\theta} \in R^q} \Delta E_1\left((\hat{\phi}, \hat{\theta}) \rightarrow \alpha\right) \quad (3.8)$$

where α is the parameter vector of the AR(K).

4 Characterization of AWJ Cut Surface

4.1 Static Characterization. Preliminary analysis of the surface profiles generated under different cutting conditions is conducted qualitatively in terms of static characteristics like R_a, R_{sk} & R_{ku}. Roughness average (R_a) of the surface profile measured at three levels is plotted against various cutting parameters in Fig. 5. It will be interesting to compare the profiles generated by AWJ with that of other manufacturing processes in terms of their shape parameters, skewness (R_{sk}) and kurtosis (R_{ku}). A diagram of skewness vs. kurtosis for various manufacturing processes is adopted from [31] and the plot of skewness vs. kurtosis for AWJ cut profiles is included (Fig. 6). From this figure, it can be noted that there is considerable overlap between the profiles generated by AWJ and that of grinding as well as EDM. This shows that AWJ is capable of generating surfaces of quality comparable to that of grinding and EDM. A value of zero for skewness (R_{sk}) and three for kurtosis (R_{ku}) is typical for a random Gaussian profile. It can be seen that the plot of R_{sk} vs. R_{ku} of AWJ profile is centered around the random Gaussian profile. Hence the profiles generated by AWJ can be defined as predominantly Gaussian in nature.

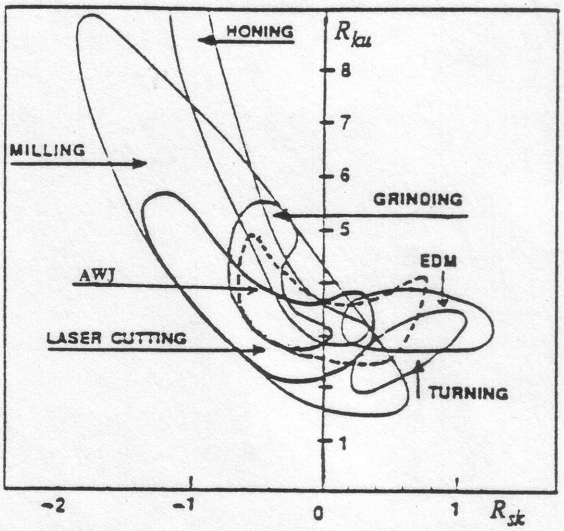

Fig. 6 Skewness / kurtosis diagram for different manufacturing processes

4.2 Dynamic Characterization. To understand more about the underlying principle of surface profile generation in jet cutting processes, we need to obtain the dynamic characteristics of the generated surface. These dynamic characteristics are in turn derived using time series analysis. Hence, the surface profile data is modeled using ARMA modeling technique. Let the surface profiles obtained be described by the following ARMA(n, n − 1) model

$$Y_t - \Phi_1 Y_{t-1} - \Phi_2 Y_{t-2} - \ldots - \Phi_n Y_{t-n} = a_t - \Theta_1 a_{t-1} - \Theta_2 a_{t-2} - \ldots - \Theta_{n-1} a_{t-n+1} \quad (4.1)$$

where, Y_t is the height of the profile at a distance t and $a_t \sim NID(0, \sigma_a^2)$.

The best fit ARMA models generated for the AWJ cut profiles range from orders ARMA(4, 3) to ARMA(2, 1). Green's function, auto co-variance function and power spectrum density of the ARMA models are computed [29] for further analysis. Typical plots of the Green's function, auto co-variance function and power spectrum density for the ARMA models fitted for the AWJ cut profile are given in Fig. 7(*a*). The peak values of Green's function, auto co-variance function and power spectrum density for different cutting conditions at the three levels are given in Table 2. Mean lag (M.Lag) indicates the lag for which the respective functions reach the mean position.

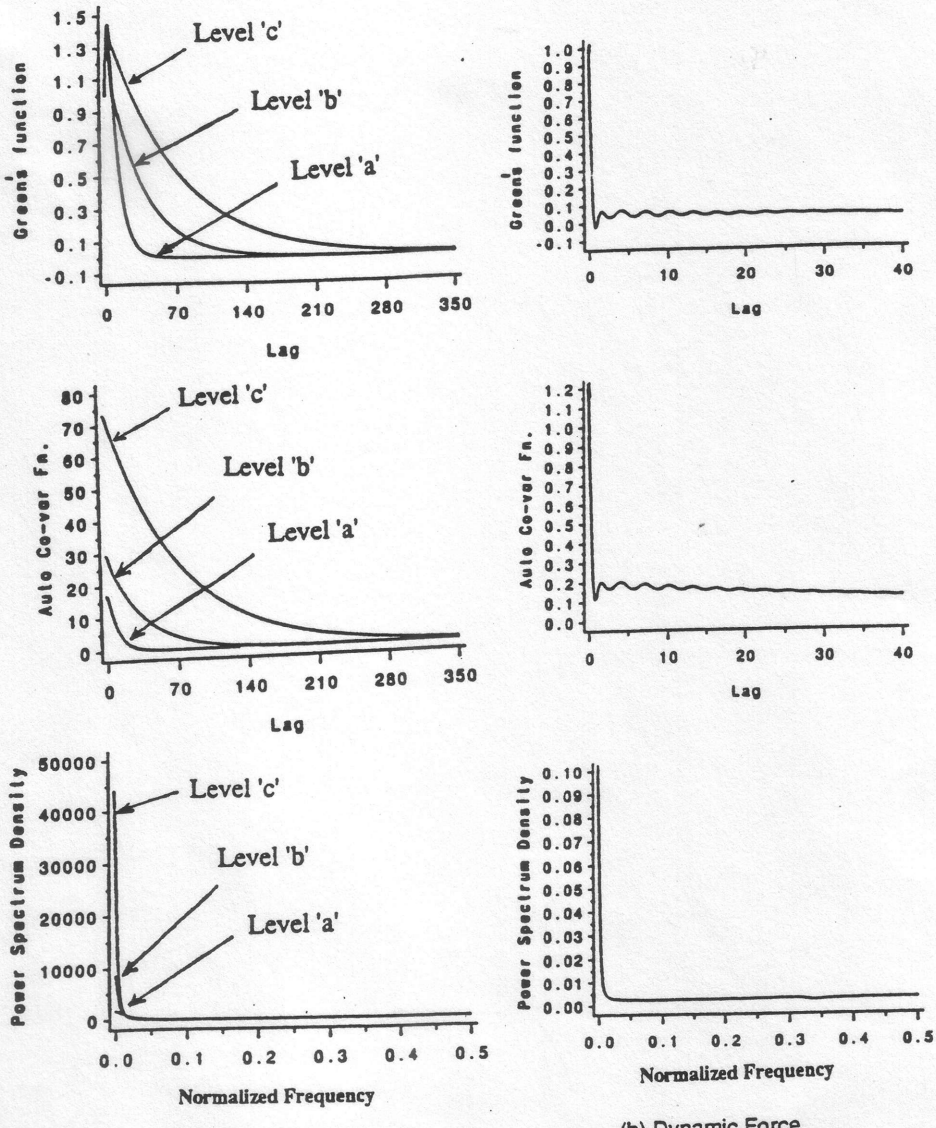

(a) Surface Profile (P=331MPa, SOD=7.62mm, V=1.27mm/s, AFR=3.22g/s)

(b) Dynamic Force (P=290 MPa, SOD=7.62mm, V=1.69 mm/s, AFR=3.22g/s)

Fig. 7 Typical plot of Green's function, auto covariance function and power spectrum density of ARMA models, (*a*) surface profile, (*b*) dynamic force

The peak values of Green's function, auto co-variance function and power spectrum density exhibit the same trend as that of surface roughness (R_a) with change in cutting parameters. As water pressure increases, R_a reduces; so do the peak values of Green's function (with one exception), auto co-variance function and power spectrum density. With increase in stand-off distance, the surface becomes smoother until a stand-off distance of about 7 mm and then it roughens. Similarly, the peak values of Green's function, auto co-variance function and power spectrum density initially reduces until a stand-off distance of 7 mm is reached and then the peak values increase. As traverse speed increases, the surface roughness (R_a) as well as the peak values of Green's function, auto co-variance function and power spectrum density increase. With increase in abrasive flow rate, the peak values of Green's function, auto co-variance function and power spectrum density have the same trend as that of change in R_a. Thus it can be concluded that Green's function, auto co-variance function and power spectrum density peaks give a well defined and quantified surface roughness value for qualitative analysis of surface profiles. They also give a common platform for comparison of different stochastic signals which can be used for process monitoring.

4.3 Wavelength Decomposition. In order to derive more information about the generated surface profile and to relate it with the cutting process in a more tangible way, it will be necessary to perform the wavelength decomposition of the roots of the ARMA models. The characteristic frequencies of the discrete roots give us the corresponding wavelengths. The relative power of the roots can be obtained from the variance decomposition. The characteristic roots of the ARMA models obtained as well as their wavelength decomposition are given in Table 3. This table also gives the break frequencies of the real roots and the damped natural frequencies of the complex roots. The relative power of the discrete roots are also given. It can be observed that all the ARMA(n, n − 1) models are asymptotically stable as they satisfy the stability criterion [29],

$$|\lambda_k| < 1, \quad k = 1, 2, \ldots, n \tag{4.2}$$

where, λ_k is a root of the model.

Table 2 System dynamics

Parameter		Surface Profile						Dynamic Force		
Water Pressure (MPa)	Level	Green's Function Peak	Green's Function M.Lag	Auto CoV. Function Peak	Auto CoV. Function M.Lag	Spectrum Density Peak		Green's Function Peak	Auto CoV Function Peak	Spectrum Density Peak
248	a	1.44@2.6	42	16.9	42	1.36E03				
	b	1.32@1.9	81	18.8	81	2.93E03				
	c	1.56@3.6		865		1.46E06		7.15E-02	2.05E-01	9.76E-02
276	a	1.41@2.5	48	17.4	48	1.54E03				
	b	1.35@2.3	108	25.8	108	4.93E03				
	c	1.52@5.5		498		6.70E05		9.37E-02	1.07E-01	8.74E-03
303	a	1.43@2.4	51	15.8	51	1.32E03				
	b	1.34@2.1	140	26.0	140	5.11E03				
	c	1.42@2.6		142		1.90E05		2.85E-03	2.90E-02	4.99E-03
331	a	1.40@2.5	55	17.2	55	1.70E03				
	b	1.38@2.3	190	29.7	190	8.78E03				
	c	1.45@2.5	360	73.3	360	4.42E04		3.53E-02	3.65E-02	2.60E-03

Parameter		Surface Profile						Dynamic Force		
Stand-off Distance (mm)	Level	Green's Function Peak	Green's Function M.Lag	Auto CoV. Function Peak	Auto CoV. Function M.Lag	Spectrum Density Peak		Green's Function Peak	Auto CoV Function Peak	Spectrum Density Peak
5.08	a	1.38@2.2	42	13.5	42	9.27E02				
	b	1.32@1.9	360	34.8	360	1.63E04				
	c	1.47@2.8		210		3.51E05		1.33E-01	2.16E-01	2.73E-02
7.62	a	1.44@2.5	65	18.6	65	1.91E03				
	b	1.40@2.2	156	26.5	156	6.04E03				
	c	1.43@2.6		92		1.17E05		5.27E-02	5.36E-02	3.54E-03
10.16	a	1.51@2.8	57	21.6	57	2.35E03				
	b	1.35@2.3	116	26.2	116	4.83E03				
	c	1.54@5.3		238		3.43E05		6.42E-02	7.21E-02	5.52E-03
12.70	a	1.53@3.0	52	23.0	52	2.31E03				
	b	1.38@2.4	105	27.5	105	4.83E03				
	c	1.60@6.6		441		1.01E06		8.26E-02	2.01E-01	6.64E-02

Parameter		Surface Profile						Dynamic Force		
Cutting Speed (mm/s)	Level	Green's Function Peak	Green's Function M.Lag	Auto CoV. Function Peak	Auto CoV. Function M.Lag	Spectrum Density Peak		Green's Function Peak	Auto CoV Function Peak	Spectrum Density Peak
0.42	a	1.42@2.3	58	15.6	58	1.41E03				
	b	No Transition Zone								
	c	1.29@1.8	95	14.5	95	2.04E03		-1.20E-01	1.12E+01	3.23E-04
0.85	a	1.36@2.3	50	14.7	50	1.18E03				
	b	1.40@2.4	100	23.0	100	3.47E03				
	c	1.38@2.2		58		3.67E04		1.00E-02	1.02E-02	2.22E-03
1.27	a	1.44@2.4	45	17.7	45	1.63E03				
	b	1.30@2.2	95	22.3	95	3.77E03				
	c	1.61@6.3		375		6.36E05		7.15E-02	1.74E-01	5.04E-02
1.69	a	1.51@2.7	55	20.6	55	2.10E03				
	b	1.35@2.0	150	31.0	150	6.61E03				
	c	1.76@10.5		605		1.19E06		1.02E+00	1.22E+00	1.06E-01

Parameter		Surface Profile						Dynamic Force		
Abrasive Fl.Rate (g/s)	Level	Green's Function Peak	Green's Function M.Lag	Auto CoV. Function Peak	Auto CoV. Function M.Lag	Spectrum Density Peak		Green's Function Peak	Auto CoV Function Peak	Spectrum Density Peak
2.27	a	1.59@2.8	56	21.8	56	2.16E03				
	b	1.46@2.7	120	28.9	120	4.87E03				
	c	2.00@11.3		865		1.86E06		2.55E-01	1.61E+00	4.15E-01
3.03	a	1.51@2.3	45	18.3	45	1.55E03				
	b	1.35@2.0	135	24.3	135	4.81E03				
	c	1.48@4.4		257		3.47E05		8.71E-02	1.01E-01	6.21E-03
3.78	a	1.40@2.5	54	17.6	54	1.73E03				
	b	1.33@2.2	121	25.8	121	5.88E03				
	c	1.54@4.1		316		5.54E05		7.06E-02	1.58E-01	3.11E-02
4.54	a	1.38@2.3	60	16.2	60	1.39E03				
	b	1.34@2.1	255	31.4	255	1.04E04				
	c	1.45@4.7		277		3.95E05		1.02E+00	1.08E+00	3.07E-02

For all cutting conditions, the primary wavelength of the model representing level "a" is of the order of one to one-and-a-half times the average size of the abrasive particles. Hence we can conclude that the surface roughness at this level is primarily caused by the abrasive particles. (Even though different sizes of abrasive particles have not been tried, it is expected that similar results will be obtained for different size abrasives too.) The fact that the primary wavelength is sometimes slightly bigger than the average size of the abrasive particles could be due to two reasons.

(*1*) The abrasive mesh size is defined by the average size of the particles. There could be a significant number of particles, above the average size, which hit the kerf wall.

(*2*) When particles impinge the surface at spacings very close to each other, the crater produced by one particle overlaps with the other such that when measured, it looks as though it is one big crater.

The secondary wavelength at level "a" is of the order of 1/3rd to half the average size of the abrasive particles. The cause for this could be attributed to the smaller size abrasive particles, improper penetration of the abrasive particles or their fragmentation. Thus, at level "a" the "waviness" (or striations) of the jet stream does not have any significant effect on the surface profile. The power of the primary wavelength is observed to be between 75 percent and 85 percent with one exception of very low traverse speed when it is 91 percent. Interestingly, all the primary as well as secondary wavelengths at level "a" have real roots except at very low traverse speed.

Level "b" is the depth of the transition zone or the depth at which the striations start to appear. So, it is expected that the effect of striations at level "b" should be evident on the wavelength decomposition. We know that the waterjet stream diverges upon exit from the mixing nozzle. Over a stand-off distance of about 8 mm, the effective diameter becomes almost double the nozzle inside diameter. In our case it becomes approximately 1.52 mm. It can be seen that, the primary wavelength at level "b" ranges from 1/3rd to one-and-a-half times the jet diameter. The power of the primary wavelength at level "b" is above 90 percent at all cutting conditions and most of them are considerably above 95 percent. This indicates the fact that the effect of jet diameter becomes more and more predominant as we go downwards along the kerf wall as expected from visual observations. The effect of secondary wavelength on the surface profile at level "b" is insignificant (as denoted by the power and magnitude) except at low stand-off distances. The secondary wavelength is about half to 1/8th the abrasive particle size except at low stand-off distance when it is twice. We can also note that the primary wavelength of all the surfaces obtained at this level has real roots. Most of the secondary wavelengths also have real roots.

Wavelength decomposition of the surface profile at level "c" indicates that the contribution of the primary wavelength is always of the order of about 99 percent of the total power. Primary wavelength of all profiles have real roots. From the studies of the mechanism of striation formation, we can show that primary wavelength at level "c" represents the influence of the AWJ stream on the surface. At lower pressures, the primary wavelength of the roots of the model representing the profile at level "c" is about three times the effective jet diameter. However, as the water pressure increases, the primary wavelength decreases and becomes almost one and a half times the effective jet diameter. The influence of stand-off distance is considerable on the primary wavelength at level "c". At lower stand-off distances it is approximately five times the effective jet diameter. But at a stand-off distance of about 7.6mm, it is only about twice the jet diameter. With further increase in stand-off distance, the primary wavelength at level "c" increases and becomes about six times the effective jet diameter. At very low traverse speeds the primary wavelength at level "c" is about 1/3rd of the jet diameter. At the traverse speed of 0.85 mm/s the primary wavelength is about one and a half times the effective jet diameter. The primary wavelength increases until it reaches about seven times the effective jet diameter. At lower abrasive flow rate, the primary wavelength is about six times the effective jet diameter. With increase in abrasive flow rate, it reduces initially; again it increases and finally reduces. This trend is expected as indicated by the change in R_a. The secondary wavelength at the deformation wear zone is about half to 1/6th the abrasive particle size. This could be attributed to the particle fragmentation rather than improper penetration. The power of the secondary wavelength is only about 1 percent at this level. Hence the effect of secondary wavelength on the surface profile can be ignored. We can see that for all cutting parameters, if the primary wavelength of the profile at level "c" is smaller, the surface will be smoother.

From this analysis we can conclude that all the cutting parameters have considerable influence on the striation generation mechanism in AWJ cutting of thick workpieces. However, in terms of surface roughness, once the optimum values

Table 3 Wavelength decomposition

Water Pressure (MPa)	Levels	Root	Discrete Roots Real	Imag.	Freq.	Power %	Wavelength (mm)
248	a	1	0.8718	0.0000	2.1830	76.60	0.2290
		2	0.6222	0.0000	6.5600	23.40	0.0762
	b	1	0.9395	0.0000	0.9932	95.23	0.5035
		2	0.3539	0.0000	16.530	4.76	0.0303
		3	-0.9655	0.0000	0.5588	0.01	0.8948
	c	1	0.9946	0.0000	0.0862	99.88	5.8020
		2	0.2957	0.2596	11.470	0.06	0.0436
		3	0.2957	-0.2596	11.470	0.06	0.0436
276	a	1	0.8951	0.0000	1.7646	83.13	0.2834
		2	0.6170	0.0000	7.6867	16.87	0.0650
	b	1	0.9555	0.0000	0.7241	96.28	0.6905
		2	0.3885	0.0000	15.048	3.72	0.0332
	c	1	0.9976	0.0000	0.1036	99.79	4.8249
		2	0.4113	0.0000	14.017	0.21	0.0357
303	a	1	0.8780	0.0000	2.0715	80.99	0.2414
		2	0.6050	0.0000	7.9969	19.01	0.0625
	b	1	0.9580	0.0000	0.6837	96.95	0.7313
		2	0.3271	0.0000	17.788	3.05	0.0281
	c	1	0.9907	0.0000	0.1487	99.98	3.3623
		2	0.5176	0.3182	8.7727	0.01	0.0570
		3	0.5176	-0.3182	8.7727	0.01	0.0570
331	a	1	0.8943	0.0000	1.7785	82.85	0.2811
		2	0.6207	0.0000	7.5894	17.15	0.0659
	b	1	0.9712	0.0000	0.4651	98.14	1.0750
		2	0.5954	0.3115	7.6715	0.93	0.0652
		3	0.5954	-0.3115	7.6715	0.93	0.0652
	c	1	0.9857	0.0000	0.2292	99.32	2.1812
		2	0.3147	0.3758	13.905	0.34	0.0360
		3	0.3147	-0.3758	13.905	0.34	0.0360

Stand-off Distance (mm)	Levels	Root	Discrete Roots Real	Imag.	Freq.	Power %	Wavelength (mm)
5.08	a	1	0.8542	0.0000	2.5089	76.02	0.1993
		2	0.6338	0.0000	7.2568	23.98	0.0689
	b	1	0.9875	0.0000	0.2002	91.50	2.4975
		2	0.6145	0.0786	2.0247	4.16	0.2470
		3	0.6145	-0.0786	2.0247	4.16	0.2470
		4	-0.1314	0.0000	32.301	0.18	0.0155
	c	1	0.9960	0.0000	0.0638	99.70	7.8383
		2	0.6145	0.3214	7.6697	0.15	0.0652
		3	0.6145	-0.3214	7.6697	0.15	0.0652
7.62	a	1	0.9046	0.0000	1.5956	86.18	0.3134
		2	0.5744	0.0000	8.8243	13.82	0.0567
	b	1	0.9651	0.0000	0.5654	98.84	0.8844
		2	0.5620	0.3428	8.7171	0.58	0.0574
		3	0.5620	-0.3428	8.7171	0.58	0.0574
	c	1	0.9904	0.0000	0.1535	99.84	3.2568
		2	0.5418	0.3650	9.4354	0.08	0.0530
		3	0.5418	-0.3650	9.4354	0.08	0.0530
10.16	a	1	0.9093	0.0000	1.5134	85.69	0.3304
		2	0.5987	0.0000	8.1643	14.31	0.0612
	b	1	0.9559	0.0000	0.7182	96.17	0.6962
		2	0.4061	0.0000	14.342	3.83	0.0349
	c	1	0.9947	0.0000	0.0843	99.45	5.9343
		2	0.4693	0.0000	12.041	0.55	0.0415
12.70	a	1	0.9073	0.0000	1.5488	83.54	0.3228
		2	0.6387	0.0000	7.1345	16.46	0.0701
	b	1	0.9558	0.0000	0.7202	96.00	0.6943
		2	0.4122	0.0000	14.104	4.00	0.0355
	c	1	0.9970	0.0000	0.0485	99.65	10.3185
		2	0.5060	0.0000	10.841	0.35	0.0461

Traverse Speed (mm/s)	Levels	Root	Discrete Roots Real	Imag.	Freq.	Power %	Wavelength (mm)
0.423	a	1	0.9042	0.0000	1.6028	91.18	0.3120
		2	0.3729	0.2388	9.0653	4.41	0.0552
		3	0.3729	-0.2388	9.0653	4.41	0.0552
	b	No Transition Zone					
	c	1	0.9394	0.0000	0.9949	98.35	0.5026
		2	0.5293	0.3583	9.4709	1.65	0.0528
		3	0.5293	-0.3583	9.4709	1.65	0.0528
0.847	a	1	0.8768	0.0000	2.0925	80.15	0.2389
		2	0.6242	0.0000	7.5007	19.85	0.0667
	b	1	0.9410	0.0000	0.9675	93.69	0.5168
		2	0.4710	0.0000	11.983	6.31	0.0417
	c	1	0.9871	0.0000	0.2067	98.75	2.4196
		2	0.5826	0.2983	7.5314	0.62	0.0664
		3	0.5826	-0.2983	7.5314	0.62	0.0664
		4	-0.4753	0.0000	11.838	0.01	0.0422
1.270	a	1	0.8988	0.0000	1.6988	85.26	0.2943
		2	0.5772	0.0000	8.7455	14.74	0.0572
	b	1	0.9510	0.0000	0.7995	95.93	0.6254
		2	0.4040	0.0000	14.425	4.07	0.0347
	c	1	0.9964	0.0000	0.0579	99.58	8.6388
		2	0.5036	0.0000	10.917	0.42	0.0458
1.693	a	1	0.9045	0.0000	1.5973	85.32	0.3130
		2	0.5895	0.0000	8.4113	14.68	0.0594
	b	1	0.9660	0.0000	0.5505	97.28	0.9082
		2	0.2511	0.0000	21.994	2.51	0.0227
		3	-0.2748	0.0000	20.558	0.21	0.0243
	c	1	0.9973	0.0000	0.0430	99.46	11.6198
		2	0.6684	0.0000	6.4119	0.54	0.0780

Abrasive Flow Rate (g/s)	Levels	Root	Discrete Roots Real	Imag.	Freq.	Power %	Wavelength (mm)
2.27	a	1	0.8979	0.0000	1.7146	82.87	0.2916
		2	0.6181	0.0000	7.6563	17.13	0.0653
	b	1	0.9498	0.0000	0.8199	94.35	0.6098
		2	0.4802	0.0000	11.675	5.65	0.0428
	c	1	0.9975	0.0000	0.0392	99.46	12.7550
		2	0.6745	0.0000	6.2682	0.54	0.0798
3.03	a	1	0.8828	0.0000	1.9840	81.10	0.2520
		2	0.6067	0.0000	7.9533	18.87	0.0629
		3	-0.6770	0.0000	6.2084	0.03	0.0805
	b	1	0.9605	0.0000	0.6414	98.66	0.7795
		2	0.2907	0.4226	15.410	0.67	0.0325
		3	0.2907	-0.4226	15.410	0.67	0.0325
	c	1	0.9956	0.0000	0.0710	99.64	7.0440
		2	0.3705	0.0000	15.805	0.36	0.0316
3.78	a	1	0.9047	0.0000	1.5943	86.23	0.3136
		2	0.5793	0.0000	8.6883	13.77	0.0575
	b	1	0.9577	0.0000	0.6879	96.65	0.7269
		2	0.3874	0.0000	15.093	3.31	0.0331
		3	-0.1550	0.8971	22.277	0.02	0.0224
		4	-0.1550	-0.8971	22.277	0.02	0.0224
	c	1	0.9961	0.0000	0.0622	99.57	8.0396
		2	0.2994	0.0000	19.194	0.37	0.0261
		3	-0.0584	0.0000	45.207	0.06	0.0111
4.54	a	1	0.8975	0.0000	1.7206	85.41	0.2906
		2	0.5765	0.0000	8.7668	14.59	0.0570
	b	1	0.9788	0.0000	0.3410	95.96	1.4661
		2	0.6226	0.2731	6.5790	2.02	0.0760
		3	0.6226	-0.2731	6.5790	2.02	0.0760
	c	1	0.9960	0.0000	0.0633	99.67	7.8976
		2	0.3950	0.0000	14.785	0.33	0.0338

of stand-off distance and abrasive flow rate are known, the surface finish can be controlled by changing traverse speed or water pressure. From the power and magnitude of the primary and secondary wavelengths, it can be inferred that as soon as the striations start appearing, the surface finish is dictated by the presence of the striations. Any parameter which improves the surface finish has a tendency to reduce the primary wavelength at the deformation wear zone. It may also be noted that as the complex roots have an exponentially decaying dynamic mode, their presence (say for a traverse rate of 0.42 mm/sec) associated with a significant power (typically greater than 1 percent) has a damping effect on the surface profile indicating a much better surface finish.

5 Characterization of Workpiece Normal Force

Information revealed by dynamic surface profile characterization can be utilized more meaningfully if they help for on-line monitoring of the surface profile. It can be noted that jet impacting force can be measured indirectly by measuring the workpiece normal force. Among the parameters that can be monitored on-line during AWJ cutting, workpiece normal force can be considered to be the most promising one for surface profile monitoring. Even though these two stochastic signals, surface profile data and dynamic force data are generated independently, characterization of the dynamic portion of the workpiece normal force through stochastic modeling will provide us a common platform for relating the surface profile with the workpiece normal force. The purpose of this investigation is to find out as to how much information can be extracted from the workpiece normal force which can be related to the surface profile generation mechanism of the AWJ cutting process.

The influence of waterjet cutting parameters on the dynamic force is studied through stochastic modeling of the force data. ARMA models are fitted for the dynamic force data produced under each cutting condition using the model distance approach. The order of the best fit ARMA models of the dynamic force signal range from ARMA(4, 3) to ARMA(2, 1). The influence of AWJ cutting parameters on the dynamic characteristics of the workpiece normal force signal is discussed below.

5.1 Influence of AWJ Cutting Parameters on Dynamic Force. Typical plots of Green's function, auto co-variance function and power spectrum density for the ARMA models fitted for the dynamic force data are illustrated in Fig. 7(*b*). Peak values of Green's function, auto co-variance function and power spectrum density are tabulated in Table 2. We can note that there is a distinct difference in trend of the Green's function of the ARMA model representing the dynamic force signal and surface profile data. From the initial value of 1.0 at G(0) for the surface profile data, the Green's function reaches a positive peak and then it drops down to the mean value; whereas for the force data, it reaches a negative peak from the initial value of 1.0 and then it stabilizes around the mean position. (This is true for all force signals except for the highest abrasive flow rate.) We can attribute the cause for the difference in behavior to the different mechanisms of stochastic signal generation. With increase in pressure, the magnitude of the peak value of Green's function reduces initially and then it increases after a pressure of 303 MPa. This behavior is similar to the trend shown by the Green's function of the profile signal at the bottom of the kerf height. The auto co-variance function also exhibits a similar trend. The power spectrum density of the dynamic force signals exhibits a similar behavior as profile signal (level "c") with increase in water pressure, i.e., it drops down continuously. This shows that the surface profile improves as pressure increases.

With increase in stand-off distance, the peak value of the Green's function reduces initially until a stand-off distance of about 7 mm and then starts increasing. Similar trend can be noticed for the peak value of the auto co-variance function. Spectrum density also exhibits a similar behavior indicating that the surface profile at 7 mm stand-off distance is the smoothest. We can see that the power spectrum of the model representing the surface profile at the bottom of kerf changes with increase in stand-off distance in the same pattern.

The peak value of the Green's function steadily increases with increase in traverse speed. However, surprisingly though the auto co-variance function peak value does not have any clear trend with increase in traverse speed. But spectrum density peak steadily increases with increase in traverse speed indicating that the surface becomes rougher. The power spectrum density of the model representing the surface profile (level "c") also exhibits the same trend with increase in traverse speed.

The Green's function or the auto co-variance function do not show any obvious trend with increase in abrasive flow rate. But, the power spectrum density peak of the workpiece normal force exhibits the same trend as that of the surface profile. It may be noted that this trend is similar to that of the surface roughness, R_a, i.e., with increase in abrasive flow rate it initially reduces then increases and finally reduces.

6 On-Line Monitoring of Surface Finish by Monitoring the Dynamic Workpiece Normal Force

From the above investigations, it can be observed that the spectral density of the ARMA model representing the workpiece normal force signal behaves the same way as that of the surface profile measurements at the bottom of the kerf (level "c") for all cutting parameters. It is interesting to note that with increase in water pressure, the roughness of the surface profile reduces; whereas the static component of the workpiece normal force increases [15]. But with increase in traverse speed the surface roughness increases; so does the static force [11, 15]. Due to this peculiarity in behavior of the static force we cannot successfully correlate the surface roughness (R_a) with static normal force. But we have seen that, the higher the PSD peak of the model representing the dynamic workpiece normal force, the higher the PSD peak of the surface profile data and the rougher the surface profile will be. Thus, the PSD peak of the model representing dynamic force data can be correlated with surface roughness very reliably.

Even though the new generation AWJ cutting system envisages the on-line control of all the four parameters, water pressure, abrasive flow rate, traverse speed and stand-off distance, only the traverse speed controller and the stand-off distance controller have been implemented. However, in practice the optimum stand-off distance and optimum abrasive flow rate which give the best surface finish for each material is determined before the actual cutting process begins. Once these parameters are known, they can be set to their pre-determined optimum value for the particular material. Thus the best in-process control parameters for surface profile monitoring will be traverse speed and water pressure. Among these two parameters, the range of surface profile that can be obtained by changing the traverse speed is much larger. However, the water pressure can be used to get a finer control of the surface finish.

Figure 8(*a*) gives a plot of the log of the power spectrum density peak of the ARMA model representing the surface profile vs. the log of the power spectrum density peak of the ARMA model representing the dynamic force with change in traverse speed. These power spectrum density peaks are derived from their respective models. The bottom left hand corner of the plot indicates the smoothest surface that can be obtained. The log of power spectrum density peak of the force has a quadratic relationship with the log of power spectrum density peak of the profile. It can be mathematically expressed as follows:

$$P = -0.10F^2 + 0.08F + 14.57 \qquad (6.1)$$

where, F – Log of power spectrum density peak of model representing dynamic force and, P – Log of power spectrum density peak of model representing surface profile. The plot of R_a vs. log of power spectrum density peak of the ARMA model representing the surface profile with change in traverse speed is shown in Fig. 8(*b*). Their relationship is given by:

$$R = 0.33P^2 - 4.43P + 19.63 \qquad (6.2)$$

where, R – Surface Roughness (R_a) and P as defined above.

Figure 8(*c*) gives a plot of the log of power spectrum density peak of the ARMA model representing the surface profile vs. the log of power spectrum density peak of the ARMA model representing the dynamic force with change in water pressure. These peaks are also derived from their respective models with the bottom left hand corner indicating the smoothest surface. Here also a quadratic relationship exists between the two variables and is mathematically given below:

$$P = -0.511F^2 - 3.252F + 9.397 \qquad (6.3)$$

where, F and P are as defined above.

The plot of R_a vs. log of power spectrum density peak of the ARMA model representing the surface profile with change in water pressure is shown in Fig. 8(*d*). Their relationship is given by:

$$R = 0.34P^2 - 6.50P + 41.69 \qquad (6.4)$$

where, R and P are as defined above.

The R_a of the kerf wall can be predicted using the relationships given by Eq. (6.1)–(6.4), once the control parameter (traverse speed or water pressure) is chosen. The predicted R_a can be compared with the desired R_a and if they are different then corresponding control signal can be sent to the AWJ cutting machine to change the chosen parameter. Thus, the PSD peak of dynamic cutting force

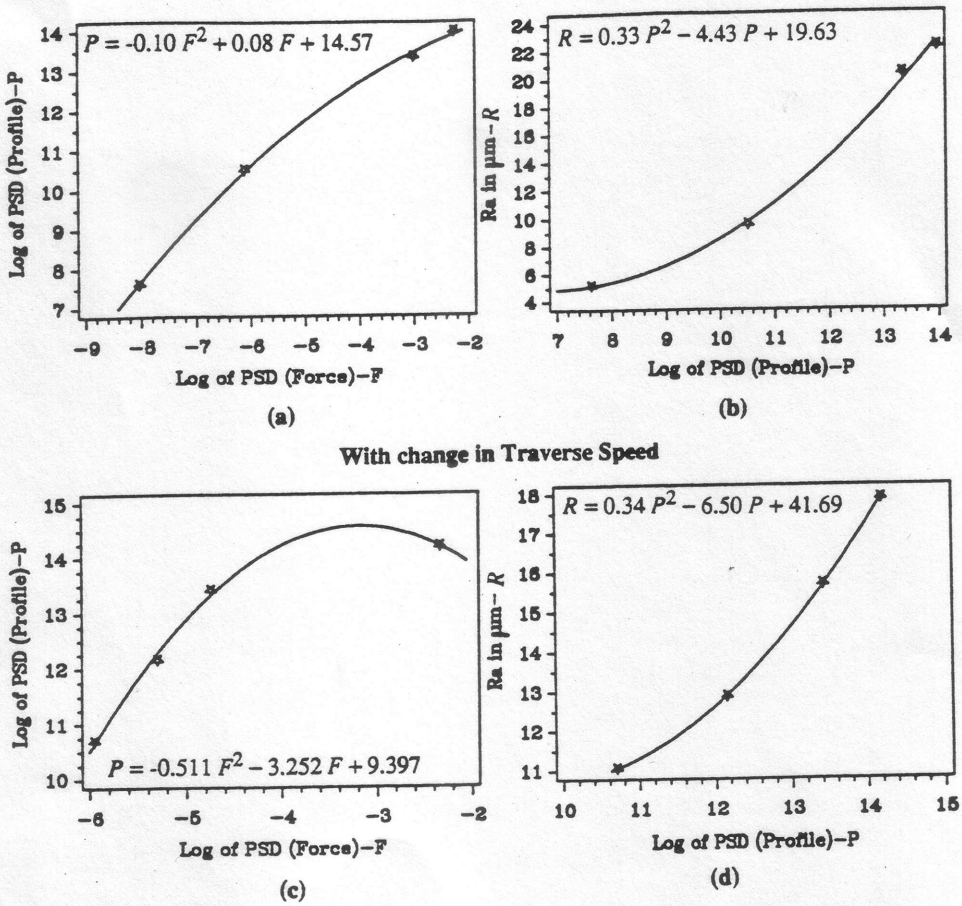

Fig. 8 *(a)* Plot of log of power spectrum density peak of ARMA model of the surface profile vs log of power spectrum density peak of ARMA model of the dynamic force with change in traverse speed, *(b)* Plot of log of power spectrum density peak of ARMA model of the surface profile vs R_a with change in traverse speed, (c) Plot of log of power spectrum density peak of ARMA model of the surface profile vs log of power spectrum density peak of ARMA model of the dynamic force with change in water pressure, *(d)* Plot of log of power spectrum density peak of ARMA model of the surface profile vs R_a with change in water pressure

signal can be used for on-line monitoring and controlling the surface roughness (R_a).

The underlying assumption here is that the workpiece material is homogeneous and that water pressure and abrasive flow rate are uniform. It may be noted that the relationships given in Fig. 8 were verified through several trials conducted under identical conditions and were found to be repeatable.

7 Conclusions

The conclusions from this investigation can be summarized as follows:

The AWJ cut surface profile is predominantly Gaussian in nature. Skewness/kurtosis diagram indicates that AWJ is capable of generating surfaces of quality comparable to grinding or EDM. Hence parameters like Green's function, auto co-variance function and/or power spectrum density which measure the dynamics of the AWJ system can be used for surface profile representation of AWJ.

Primary and secondary wavelengths are responsible for the surface profile of AWJ cut surfaces. The power of the primary wavelength at the cutting wear zone is about 75 percent to 85 percent. The primary and the secondary wavelength at the cutting wear zone are caused by the abrasive particles. At this zone, the "waviness" of the jet stream does not have any significant effect on the surface profile. The power of the primary wavelength is above 90 percent at the transition zone. Primary wavelength at the transition zone is caused by the jet stream and the secondary wavelength is caused by the abrasive particles. Primary wavelength ranges from 1/3rd to about one-and-a-half times the jet diameter. The contribution of the primary wavelength in the deformation wear zone is about 99 percent of the total power. This wavelength varies from 1/3rd to about seven times the effective jet diameter. The secondary wavelength in the deformation wear zone is about half to 1/6th the average abrasive particle size. Any parameter which improves surface finish has a tendency to reduce the primary wavelength at the deformation wear zone.

The spectral density of the ARMA model of the dynamic force behaves the same way as that of the surface profile measurements at the deformation zone for all cutting parameters. The peak of the power spectrum density of the ARMA models representing the dynamic workpiece normal force signal can be considered as a potential parameter for on-line monitoring of the surface finish at the deformation wear zone.

Acknowledgments

The authors would like to thank the Center for Robotics and Manufacturing Systems, University of Kentucky, for the financial support in executing this project and Flow International Inc., Kent, Washington, for providing the AWJ cutting system.

References

1 Tan, D. K. M., 1986, "A Model for the Surface Finish in Abrasive Waterjet Cutting," *8th International Symp. on Jet Cutting Technology*, England, 9–11 Sept., Paper 31, pp. 309–313.

2 Hashish, M., 1989, "Advanced Machining with Abrasive Waterjets —Theory and Applications," *Proceedings of Non-Traditional Machining Conference of SME*, Oct. 30–Nov. 2, pp. 1–45.

3 Webb, K. E., and Rajurkar, K. P., 1990, "Surface Characterization of Inconel Cut by Abrasive Waterjet," *Proceedings of CSME Mechanical Engineering Forum*.

4 Hashish, M., 1991, "Characteristics of Surfaces Machined with Abrasive-Waterjets," ASME *Journal of Engineering Materials and Technology*, Vol. 113, July, pp. 354–362.

5 Kovacevic, R., Liaw, H. H., and Barrows, J. F., 1988, "Surface Finish and its Relationship to Cutting Parameters," *Proceedings of 3rd Intl. Grinding Conference*, MR88-589, pp. 1–15.

6 Kovacevic, R., 1991, "Surface Texture in Abrasive Waterjet Cutting," *The SME's Journal of Manufacturing Systems*, Vol. 10, No. 1.

7 Hashish, M., 1988, "Visualization of the Abrasive Waterjet Cutting Process," *Experimental Mechanics*, June, pp. 159–169.

8 Chao, J., Geskin, E. S., and Chung, Y., 1992, "Investigation of the Dynamics of the Surface Topography Formation during Abrasive Waterjet Machining," *Proceedings of the 11th International Conference on Jet Cutting Technology*, 8–10, Sept., St. Andrews, Scotland, pp. 593–603.

9 Hashish, M., 1992, "On the Modeling of Surface Waviness Produced by Abrasive-Waterjets," *Proceedings of the 11th International Conference on Jet Cutting Technology*, 8–10, Sept., St. Andrews, Scotland, pp. 17–34.

10 Mohan, R., Kovacevic, R., and Zhang, Y. M., 1992, "Characterization of Surface Texture Generated by High Energy Jets," *Proceedings of the ASME Winter Annual Meeting*, Nov. 8–13, Anaheim, CA, PED-Vol. 62, pp. 203–218.

11 Hunt, D. C., Burnham, C. D., and Kim, T. J., 1987, "Surface Finish Characterization in Machining Advanced Ceramics by Abrasive Waterjet," *Proceedings of the 4th U.S. Waterjet Conference*, Berkeley, CA, Aug.

12 Hunt, D. C., Kim, T. J., and Reuber, M., 1988, "Surface Finish Optimization for Abrasive Waterjet Cutting," *9th International Symp. on Jet Cutting Technology*, Oct., Paper C1, pp. 99–112.

13 Burnham, C. D., and Kim, T. J., 1989, "Statistical Characterization of Surface Finish Produced by a High Pressure Abrasive Waterjet," *Proceedings of 5th American Waterjet Conference*, Aug. 29–31, Canada, Paper 16, pp. 165–175.

14 Curhan, J., Reuber, M., and Kim, T. J., 1989, "Force Control of Surface Finish in Abrasive Waterjet Cutting," *Proceedings of the ASME WAM*, San Francisco, CA, Dec. 10–15, PED Vol. 41, pp. 31–36.

15 Kovacevic, R., and Beardsley, H. E., 1990, "On Line Monitoring the Quality of the Surface Cut by the Abrasive Waterjet," *Proc. of the 4th Intl. Grinding Conference*, Oct. 9–11, Dearborn, MI, MR90-535, pp. 1–10.

16 Whitehouse, D. J., Vanherck, P., De Bruin, W., and Luttervelt Van, C. A., 1974, "Assessment of Surface Typology Analysis Techniques in Turning," *Annals of the CIRP*, Vol. 23, No. 2, pp. 265–282.

17 O'Conner, R. F., and Spedding, T. A., 1992, "The Use of Complete Surface Profile Description to Investigate the Cause and Effect of Surface Features," *International Journal of Machine Tools Manufacturing*, Vol. 32, No. 1/2, pp. 147–154.

18 Peters, J., Vanherck, P., and Sastrodinoto, M., 1979, "Assessment of Surface Typology Analysis Techniques," *Annals of the CIRP*, Vol. 28, No. 21, pp. 539–554.

19 Pandit, S. M., Nassirpour, F., and Wu, S. M., 1977, "Stochastic Geometry of Anisotropic Random Surfaces with Application to Coated Abrasives," ASME JOURNAL OF ENGINEERING FOR INDUSTRY, Feb., Vol. 99, pp. 218–224.

20 Wu, S. M., 1977, "Dynamic Data System—A New Modeling Approach," ASME JOURNAL OF ENGINEERING FOR INDUSTRY, Aug., Vol. 99, pp. 708–714.

21 Radhakrishnan, T., and Wu, S. M., 1981, "On-line Hole Quality Evaluation for Drilling Composite Material using Dynamic Data," ASME JOURNAL OF ENGINEERING FOR INDUSTRY, Vol. 103, Feb., pp. 119–125.

22 Wu, S. M., and Ungpiyakul, T., 1980, "New Applications of Dynamic Data System (DDS) Methodology," *Proceedings of ASM Process Modeling Session*, Materials and Process Congress, Cleveland, OH, pp. 23–37.

23 Pandit, S. M., and Revach, S., 1981, "A Data Dependent System Approach to Dynamics of Surface Generation Turning," ASME JOURNAL OF ENGINEERING FOR INDUSTRY, Vol. 103, Nov., pp. 437–445.

24 Williams, R. E., and Rajurkar, K. P., 1991, "Study of Wire Electrical Discharge Machined Surface Characteristics," *Computer Aided Production Engineering*, Elsevier, pp. 127–138.

25 Rajurkar, K. P., and Bhatia, S. K., 1990, "Investigation of Surface Characteristics in Electrochemical Grinding," *ASME Manufacturing International '90*, special volume, pp. 119–124.

26 Williams, R. E., and Rajurkar, K. P., 1992, "Stochastic Modeling and Analysis of Abrasive Flow Machining," ASME JOURNAL OF ENGINEERING FOR INDUSTRY, Vol. 114, Feb., pp. 74–81.

27 Pandit, S. M., and Shunmugam, M. S., 1992, "Signature of Machine Tool Errors on Surface Texture by DDS," ASME JOURNAL OF ENGINEERING FOR INDUSTRY, Vol. 114, Feb., pp. 370–374.

28 Kovacevic, R., and Zhang, Y. M., 1992, "Identification of Surface Characteristics from Large Samples," *Proceedings of the Institute of Mechanical Engineers, Part C, Journal of Mechanical Engineering Science*, Vol. 206, pp. 275–284.

29 Pandit, S. M., and Wu, S. M., 1983, *Time Series and System Analysis with Applications*, John Wiley & Sons, New York.

30 Box, G. E. P., and Jenkins, G. M., 1976, *Time Series Analysis, Forecasting & Control*, Holden Day, CA.

31 Bedrin, C., Yuan, S. F., and Querry, M., 1988, "Investigation of Surfaces Microgeometry in Laser Cutting," *Annals of the CIRP*, Vol. 37, No. 1.